

# Calibration Effects for Laser-Induced Breakdown Spectroscopy of Gaseous Sample Streams: Analyte Response of Gas-Phase Species versus Solid-Phase Species

V. Hohreiter and D. W. Hahn\*

Department of Mechanical and Aerospace Engineering, University of Florida, Gainesville, Florida 32611

The effects of analyte phase on the calibration response for laser-induced breakdown spectroscopy is investigated for a range of carbon species. Significant differences in the atomic emission signal from carbon were observed when comparing calibration streams of gas-phase and submicrometer-sized solid-phase carbon species. The resulting calibration curve slopes varied by a factor of 8 over a comparable range of atomic carbon concentrations for five different analyte sources, while the plasma electron density and temperature remained essentially constant. The current findings challenge a widely held assumption that complete dissociation of constituent species within a highly energetic laser-induced plasma results in independence of the analyte atomic emission signal on the analyte source. A physical model of the plasma–analyte interaction is proposed that provides a framework to account for the observed dependence on the physical state of the analyte.

Since the early 1980s, the use of laser-induced breakdown spectroscopy (LIBS) has steadily increased as a quantitative analytical technique, with applications to a wide range of solids, liquids, gases, and aerosols.<sup>1–3</sup> In recent studies, LIBS has been used in conjunction with single-shot analysis to effectively sample and analyze aerosol populations using discrete particle analysis.<sup>4–6</sup> In other applications, LIBS-based sensing has been successfully implemented for continuous on-line monitoring of air emissions and aerosols<sup>7–11</sup> and for analysis of ambient air particulate

matter.<sup>4,12,13</sup> More recent studies have addressed the feasibility of LIBS for analysis of biological materials and bioaerosols.<sup>14–17</sup> Important research issues regarding LIBS-based analysis of gaseous sample streams, notably aerosol detection and single-particle analysis, include the overall analyte sensitivity, precision, sampling methodology, and calibration schemes.

Calibration has been an important issue since Radziemski et al. first demonstrated the viability of LIBS for detection of atomic species from aerosol samples.<sup>18</sup> In their landmark study, beryllium-rich aerosols were generated by either laser ablation or produced by a nebulizer/heat chamber system, with the latter used for generation of calibration curves and subsequent calculation of detection limits. A different nebulizer was used in a continuing study, which produced aerosols estimated to be in the submicrometer size range.<sup>19</sup> Calibration curves were generated for three analytes, namely, cadmium, lead, and zinc, and were characterized by initial linearity followed by various degrees of saturation at higher concentrations. The saturation effects were attributed to incomplete vaporization of particles. An important finding was the general agreement (within 10%) of lead atomic emission signals of comparable atomic lead concentrations when nebulizing either lead acetate, lead chloride, or lead nitrate. Cadmium revealed a 27% difference in analyte response when comparing nebulized solutions of cadmium nitrate and cadmium chloride. In experiments analogous to the aerosol studies, the relative independence of analyte signals on molecular source for purely gas-phase species was reported in several studies.<sup>20,21</sup> Specifically, Dudragne et al. demonstrated that analyte signals for fluorine, chlorine, sulfur,

\* To whom correspondence should be addressed. E-mail: dwhahn@ufl.edu. Telephone: 352-392-0807. Fax: 352-392-1071.

- (1) Rusak, D. A.; Castle, B. C.; Smith, B. W.; Winefordner, J. D. *Crit. Rev. Anal. Chem.* **1997**, *27*, 257–290.
- (2) Sneddon, G. J.; Lee, Y.-I. *Anal. Lett.* **1997**, *32*, 2143–2162.
- (3) Lee, W. B.; Wu, J. Y.; Sneddon, J. *Appl. Spectrosc. Rev.* **2004**, *39*, 27–97.
- (4) Hahn, D. W. *Appl. Phys. Lett.* **1998**, *72*, 2960–2962.
- (5) Hahn, D. W.; Lunden, M. M. *Aerosol Sci. Technol.* **2000**, *33*, 30–48.
- (6) Carranza, J. E.; Iida, K.; Hahn, D. W. *Appl. Opt.* **2003**, *42*, 6022–6028.
- (7) Zhang, H.; Yueh, F. Y.; Singh, J. P. *Appl. Opt.* **1999**, *38*, 1459–1466.
- (8) Neuhauser, R. E.; Panne, U.; Niessner, R.; Wilbring, P. *Fresenius J. Anal. Chem.* **1999**, *364*, 720–726.
- (9) Neuhauser, R. E.; Panne, U.; Niessner, R.; Petrucci, G. A.; Cavalli, P.; Omenetto, N. *Anal. Chim. Acta* **1997**, *346*, 37–48.
- (10) Nunez, M. H.; Cavalli, P.; Petrucci, G.; Omenetto, N. *Appl. Spectrosc.* **2000**, *54*, 1805–1816.
- (11) Ferioli, F.; Puzinauskas, P. V.; Buckley, S. G. *Appl. Spectrosc.* **2003**, *57*, 1183–1189.

- (12) Carranza, J. E.; Fisher, B. T.; Yoder, G. D.; Hahn, D. W. *Spectrochim. Acta, Part B* **2001**, *56*, 851–864.
- (13) Lithgow, G. A.; Robinson, A. L.; Buckley, S. G. *Atmos. Environ.* **2004**, *38*, 3319–3328.
- (14) Morel, S.; Leone, N.; Adam, P.; Amouroux, J. *Appl. Opt.* **2003**, *42*, 6184–6191.
- (15) Samuals, A. C.; DeLucia, F. C.; McNeisby, K. L.; Miziolek, A. W.; *Appl. Opt.* **2003**, *42*, 6205–6209.
- (16) Boyain-Goitia, A. R.; Beddows, D. C. S.; Griffiths, B. C.; Telle, H. H. *Appl. Opt.* **2003**, *42*, 6119–6132.
- (17) Hybl, J. D.; Lithgow, G. A.; Buckley, S. G. *Appl. Spectrosc.* **2003**, *57*, 1207–1215.
- (18) Radziemski, L. J.; Loree, T. R.; Cremers, D. A.; Hoffman, T. M. *Anal. Chem.* **1983**, *55*, 1246–1252.
- (19) Essien, M.; Radziemski, L. J.; Sneddon, J. J. *Anal. At. Spectrom.* **1988**, *3*, 985–988.
- (20) Dudragne, L.; Ph. Adam, Amouroux, J. *Appl. Spectrosc.* **1998**, *52*, 1321–1327.

and carbon scaled with the number of respective atoms in the constituent molecules for a wide range of compounds, concluding that the parent molecules were fully dissociated in the laser-induced plasma.<sup>20</sup> Tran et al. verified that SF<sub>6</sub> and HF yielded essentially identical fluorine atomic emission signals when the gas composition was adjusted to contain the same atomic fluorine mole fraction.<sup>21</sup>

The above comments support a widely used assumption within the LIBS community, namely, that complete dissociation of constituent species within the highly energetic laser-induced plasma results in independence of the analyte atomic emission signal on the analyte source. This statement of independence of analyte source must be clearly distinguished from the presence of plasma matrix effects. Plasma matrix effects are considered changes in a specific analyte emission response due to interactions with or perturbations of the plasma, such as changes in plasma temperature, quenching of atomic emission lines by other species, or loss of an emitting species due to recombination with other atoms. For example, Gleason and Hahn observed temporal-dependent changes in mercury atomic emission as the overall gas composition of the laser-induced plasma was varied.<sup>22</sup> The distinction between analyte source effects and plasma matrix effects is significant, because when one considers the latter, there is generally an accepted temporal starting point where the atomic concentrations are considered to reflect a matrix-independent baseline. Such a constant temporal starting point was observed with mercury emission as the gas matrix was varied in the study by Gleason and Hahn, noting that the analyte source was held constant.<sup>22</sup> Notwithstanding the apparent de facto acceptance of analyte signal independence on analyte source for laser-induced plasma spectroscopy, to date no studies have systematically examined this issue for LIBS-based analysis of gaseous and aerosol-laden streams.

As the LIBS-based analysis of increasingly complex gas-phase and aerosol systems becomes more prevalent, high accuracy and precision become increasingly important. Therefore, precise calibration of the analyte signal response is required, as the number of factors contributing to the emission signal (i.e., laser parameters, optical configuration, spectrometer/detector, and plasma matrix) is sufficiently large to render an a priori calculation of analyte signal response impractical. LIBS calibration schemes are made more difficult when the systems of interest include complex and unknown analyte compositions (i.e., mixtures of gas-phase and particulate-phase analyte species), which may exist for ambient air or combustion effluent streams. For example, carbon in ambient air is present as carbon dioxide at several hundred ppm, but is generally present as fine particulate matter (such as soot), and within biological particles such as pollens and bacterial spores. Similarly, metal species at moderate to high temperatures may exist as vapor-phase species and also as homogeneously or heterogeneously nucleated particulates. Given the inherent assumption of complete dissociation of analyte species, most calibration schemes to date have focused on a precise and accurate means of analyte introduction, not on the resulting physical state of the analyte. As described above, the use of purely gaseous analyte species and the nebulization of aqueous solutions are the

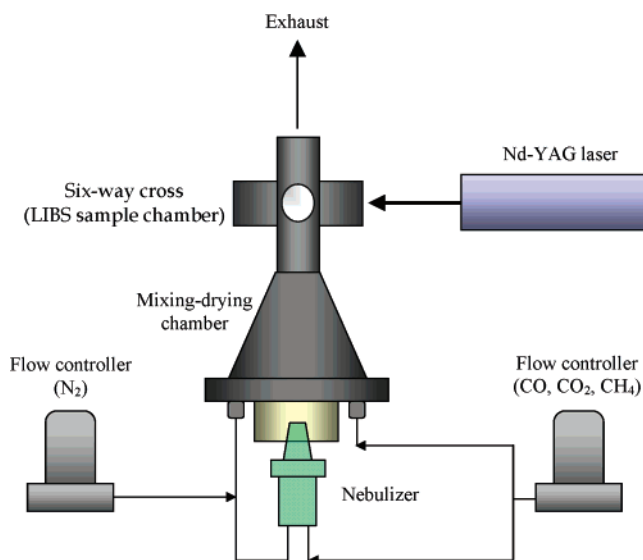


**Figure 1.** Schematic of the experimental apparatus.

most widely used calibration schemes with LIBS, noting that the former produces a homogeneous-phase (i.e., all gaseous) source for laser-induced breakdown, while the latter produces a well-dispersed, high number density mixture of generally micrometer-to submicrometer-sized aerosols in the gas matrix. The present study examines the phenomena of analyte dissociation and analyte emission for different sources (both gas phase and solid phase) of atomic carbon and the resulting effects on analyte calibration response.

## EXPERIMENTAL METHODS

The experimental system used in the current study has been reported in detail previously<sup>23</sup> and is briefly described here. For all experiments, a 1064-nm Q-switched Nd:YAG laser running at a 5-Hz repetition rate, 10-ns pulse width, and 290 mJ/pulse was focused using a 50-mm-diameter, 75-mm-focal length lens to create the plasma. The plasma emission was collected on-axis with a pierced mirror and fiber-coupled to a 0.275-m spectrometer with a 2400 groove/mm grating (0.12-nm optical resolution). Spectral data were recorded using an iCCD detector array. All carbon emission spectra were recorded using a delay of 10  $\mu$ s with respect to the incident laser pulse and a signal integration time of 12  $\mu$ s. This detector gating optimized the analyte signal of interest, namely, the carbon(I) line at 247.86 nm. Additional H $\alpha$  (656 nm) emission spectra were recorded using a temporal delay of 4  $\mu$ s and a gate width of 4  $\mu$ s, while CN and N<sub>2</sub><sup>+</sup> emission spectra were recorded using a temporal delay of 40  $\mu$ s and a gate width of 60  $\mu$ s.

Five different carbon-containing species were introduced to the LIBS sample chamber, as shown in Figure 1, with the goal of providing different physical and chemical states of the carbon carrier species. Calibration stream flow rates and analyte concentrations were adjusted to provide a comparable range of atomic carbon mass concentrations for all experiments.

**Solid-Phase Carbon Experiments.** Two different types of solutions were nebulized to provide a carbon-rich aerosol stream

(21) Tran, M.; Smith, B. W.; Hahn, D. W.; Winefordner, J. D. *Appl. Spectrosc.* **2001**, *55*, 1455–1461.

(22) Gleason, R. L.; Hahn, D. W. *Spectrochim. Acta, Part B* **2001**, *56*, 419–430.

(23) Hahn, D. W.; Carranza, J. E.; Arsenault, G. R.; Johnsen, H. A.; Hencken, K. *Rev. Sci. Instrum.* **2001**, *72*, 3706–3713.

(i.e., solid-phase analyte) to the LIBS sample chamber. For the first set of experiments, carbon solutions were prepared in the range from 500 to 5000  $\mu\text{g}/\text{mL}$  atomic carbon by dilution of atomic absorption (AA) and inductively coupled plasma-atomic emission spectroscopy (ICP-AES) grade carbon standard solutions (SPEX CertiPrep, 10 000  $\mu\text{g}/\text{mL}$  carbon as oxalic acid,  $(\text{COOH})_2$ ). For the second set of experiments, carbon solutions were prepared in a similar mass concentration range using a monodisperse particle suspension of 30-nm polystyrene ( $\text{C}_8\text{H}_8$ ) spheres (Duke Scientific). To avoid foaming within the nebulizer, the polystyrene suspensions were first washed with a resin (Bio-Rad, AG 501-X8, 20–50 mesh, Molecular Biology Grade) to remove the surfactant. Specifically, 50 g of twice-washed resin was added to 300 mL of the polystyrene suspension (1% solids) and stirred for 18 h, after which the polystyrene suspension was poured off. For all experiments, the carbon mass concentration for the polystyrene suspensions was adjusted by dilution with ultrapurified deionized (DI) water, using the manufacturer's initial specification (10% solids). The exact mass loadings were then verified by evaporating the water and weighing the remaining dried polystyrene mass corresponding to a known initial suspension volume. The preliminary estimates of carbon concentration based on the manufacturer's mass loadings and the measured mass loadings agreed to within 5%, with the small difference attributed to the loss of some particles to the resin beads during surfactant removal.

Aerosol flows were generated using a pneumatic nebulizer supplied with 5 L/min dry nitrogen. A 46 L/min dry nitrogen coflow was introduced to the aerosol stream to ensure uniform bulk flow and to facilitate complete desolvation of the nebulizer droplets, resulting in primarily submicrometer-sized aerosol particles at the LIBS sample point, as shown in Figure 1. For the given flow scheme,  $\sim 10^3$  particles exist in any given plasma volume based on the expected plasma volume and aerosol loading. The nitrogen supply was HEPA filtered prior to use, and all gases were metered with precision mass flow controllers. Prior to nebulization, the polystyrene suspensions were well mixed and then sonified for 5 min to minimize any particle agglomeration. The overall aerosol generation system was described in full detail in a previous publication,<sup>23</sup> where nebulization of similar AA-ICP standard solutions provided aerosols with a modal diameter less than 100 nm based on particle sampling and transmission electron microscopy (TEM) analysis.

The total mass loading of carbon in the LIBS sample stream was defined by the liquid nebulization rate (nominally 0.12 mL/min), the carbon mass concentration in the liquid solution/suspension, and the total gas flow rate (nebulizer flow plus coflow). The solution/suspension concentrations were adjusted to provide a nominal range from 1000 to 10 000  $\mu\text{g}/\text{m}^3$  through the LIBS sample chamber, which corresponds to about 900–9000 parts per billion (ppb) elemental carbon on a mass basis.

**Gas-Phase Carbon Experiments.** Three different carbon-containing gaseous species were used to provide a carbon-rich sample stream (i.e., gas-phase analyte) to the LIBS sample chamber. The three gas-phase species, carbon dioxide, carbon monoxide, and methane, were purchased as nominally 50 ppm mixtures in a dry nitrogen balance (Spectra Gases). The actual concentrations ranged from 49.3 to 50.8 ppm, with the true concentrations used for all calculations. The gases were metered

with precision mass flow controllers and mixed with the nitrogen coflow gas stream to provide a range of carbon mass loadings consistent with the values used for the solid-phase experiments. To provide consistency with the solid-phase experiments, the nebulizer was operated with ultrapurified deionized water, and the total gas flow rate was maintained at the same value for all experiments. In addition, valves on the experimental apparatus allowed the analyte gas streams ( $\text{CO}$ ,  $\text{CO}_2$ ,  $\text{CH}_4$ ) to be diverted through the nebulizer for the case of 5 L/min analyte gas flow rate.

The total mass loading of carbon in the LIBS sample stream was controlled by adjusting the relative flow rates of the analyte gas stream and the nitrogen coflow stream. The experimental conditions were adjusted to provide a nominal range from 1000 to 7800  $\mu\text{g}/\text{m}^3$  through the LIBS sample chamber.

**LIBS Data Collection.** The analyte peak of interest was the carbon(I) atomic emission line at 247.86 nm (21 648–61 982  $\text{cm}^{-1}$ ). The recorded spectral window was  $\sim 30$  nm wide (230–260 nm) and was nominally centered on the 247-nm carbon line. For each carbon species and carbon mass concentration, a series of 6000 spectra ( $6 \times 1000$  shots) were recorded and ensemble-averaged. The experiments were repeated between four and eight times for each carbon species, with each experiment recorded on different days in an attempt to average any fluctuations in the overall system. Spectra were also recorded for the nebulization of DI water only for all experiments to serve as spectral blanks (i.e., no carbon emission line).

In addition to data recorded near the 247-nm carbon line, emission spectra were also collected for each experimental condition, including DI water only, using 30-nm spectral windows centered at 656 and 385 nm to capture emission features corresponding to the  $\text{H}_\alpha$  atomic emission line and the cyanide and  $\text{N}_2^+$  molecular emission bands, respectively. Free electron densities were measured from the Stark broadening of the 656-nm  $\text{H}_\alpha$  line using the same procedures reported recently.<sup>24,25</sup> Briefly, following the work of Griem, the  $\text{H}_\alpha$  line intensities at full width half-maximum were related to the electron density using the fractional half-widths of the reduced Stark profile.<sup>26</sup>

## RESULTS

Representative spectra in the range of the 247-nm carbon line are shown in Figure 2 for both gas-phase and solid-phase carbon sources. For discussion purposes, the nebulized AA and ICP-AES grade carbon standard solutions will be referred to as the AA-ICP case, the nebulized 30-nm polystyrene suspensions will be referred to as the 30-nm PS case, and the three gas-phase experiments will be referred to as the  $\text{CO}_2$ ,  $\text{CO}$ , and  $\text{CH}_4$  cases. The upper set of four spectra represents the unprocessed plasma emission as recorded, demonstrating the presence of the carbon atomic emission line in combination with significant continuum emission. The lower set of three spectra represents background-subtracted spectra, which are characterized by the presence of the distinct carbon emission line and an essentially zero baseline. The baseline-corrected spectra were obtained by scaling the

(24) Carranza, J. E.; Hahn, D. W. *Spectrochim. Acta, Part B* **2002**, *57*, 779–790.

(25) Hohreiter, V.; Carranza, J. E.; Hahn, D. W. *Spectrochim. Acta, Part B* **2004**, *59*, 327–333.

(26) Griem, H. R. *Spectral Line Broadening by Plasmas*; Academic Press: New York, 1974.

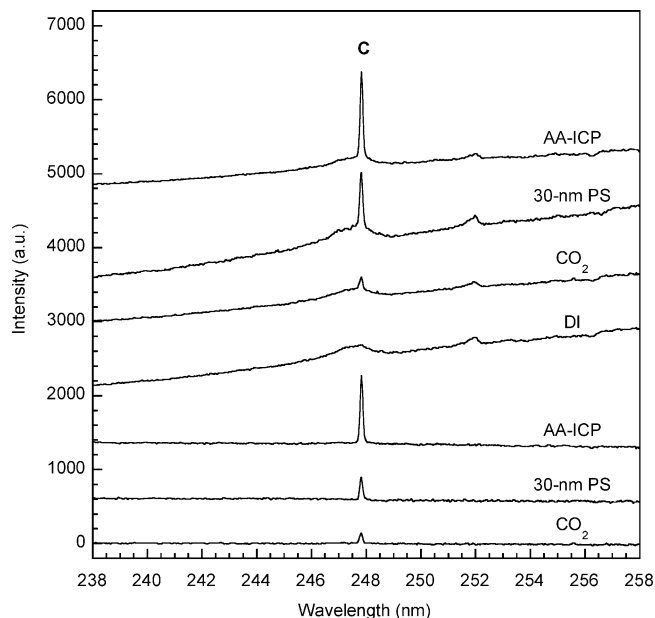


**Figure 2.** LIBS spectra in the vicinity of the 247.86-nm carbon atomic emission line for different sources of carbon. The upper four spectra represent raw data, the lower three curves are background-subtracted spectra using the deionized water spectrum (DI) as a blank. All spectra have the same scale and have been shifted vertically for clarity.

average DI water-only spectrum (also shown in Figure 2) to the carbon-containing spectrum of interest for each data set and then subtracting the scaled background. This process was very successful in removing the continuum emission, as evidenced in Figure 2 by the flat spectral response surrounding the distinct, isolated carbon emission peak.

The carbon signal used for this study was the calculated peak-to-base (P/B) ratio. This metric provides a precise measure of laser-induced plasma atomic emission by normalizing out fluctuations in the absolute plasma emission signal.<sup>18,24</sup> The reported P/B ratio was calculated using the integrated full peak area of the 247-nm carbon emission line divided by the integrated signal of the scaled background spectrum over the same spectral width.

Using this procedure, calibration curves were calculated over the range of carbon mass concentrations for each of the carbon analyte sources. The resulting calibration curves are presented in Figure 3 for all five analyte sources. All five curves display high linearity, with the slopes and corresponding regression coefficients summarized in Table 1. However, despite the constant experimental conditions and similar range of atomic carbon mass loadings for all five species, the resulting slopes of the calibration curves reveal marked differences. Most significantly, the calibration slope for the AA-ICP standard was roughly double that of the 30-nm PS curve and eight times that of the three gas-phase species curves. Consistent with previous findings, the three gas-phase calibration curves group very closely to one another, with the differences in slope being statistically insignificant. In addition, experiments for the three gas-phase species were repeated at discrete data points with the carbon-containing gas stream fed through the nebulizer. This exercise did not reveal any significant changes in the resulting P/B ratios with respect to the Figure 3 data, confirming that nebulization of the analyte species is not responsible for the marked difference in analyte response between

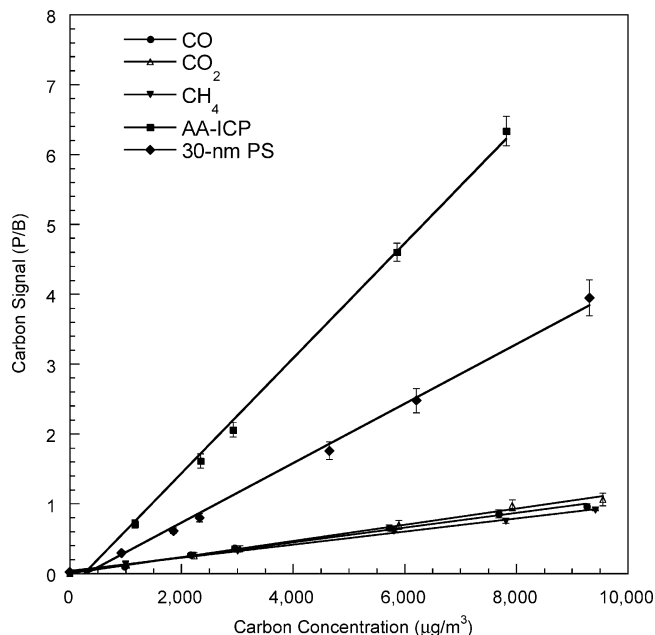


**Figure 3.** Calibration curves based on the 247.86-nm C atomic emission line for the five carbon analyte sources investigated. Error bars represent one standard deviation.

**Table 1. Summary of the Carbon Calibration Response and Plasma Conditions**

analyte source	calib curve slope (%)	calib curve <i>R</i> value	free elec density ( $10^{17} \text{ cm}^{-3}$ ) (%)	plasma temp (K)	CN signal (P/B)
DI blank	n/a <sup>a</sup>	n/a	$1.06 \pm 4.4$	$5190 \pm 80$	n/a
AA-ICP	$8.24 \times 10^{-4} \pm 5.2$	0.999	$1.03 \pm 4.6$	$4970 \pm 10$	22.3
30-nm PS	$4.25 \times 10^{-4} \pm 5.8$	0.998	$1.06 \pm 4.4$	$4800 \pm 100$	15.0
CO	$1.05 \times 10^{-4} \pm 9.6$	0.997	$1.04 \pm 4.5$	$4950 \pm 40$	6.98
CO <sub>2</sub>	$1.16 \times 10^{-4} \pm 3.2$	0.997	$1.00 \pm 4.7$	$5110 \pm 20$	6.07
CH <sub>4</sub>	$9.38 \times 10^{-5} \pm 4.2$	0.998	$1.06 \pm 4.4$	$4990 \pm 70$	10.2

<sup>a</sup> n/a, not applicable.

the gas-phase and solid-phase carbon species. Clearly, the current results contradict the assumption of analyte signal independence on the analyte source when one considers both solid-phase and gaseous-phase analyte sources, or even between varying sized solid-phase analyte sources. Prior to further analysis and discussion of the observed analyte source effect, it is useful to consider possible changes in the plasma itself (i.e., true matrix effects).

Although care was taken to provide a consistent overall matrix for all experiments, including the nebulization of DI water for all cases, it is necessary to examine whether the different analyte species had any effect on the bulk plasma. For example, large variations in plasma properties, such as electron density and temperature, resulting from the different analyte species could explain the different analyte response curves. One measure of consistent plasma formation is the continuum plasma emission. Careful examination of the Figure 2 data reveals identical background-subtracted spectra in the region about the carbon emission peak. This was also the case for the remaining analyte sources, namely, CO and CH<sub>4</sub>. Based on the consistent shape of the plasma continuum emission between the DI water case and all five analyte cases, one may conclude similar plasma properties, namely, temperature. However, to provide a more quantitative

measure of plasma consistency, the free electron densities, from the measurements of  $H_{\alpha}$  line Stark broadening, were also evaluated. The fractional half-widths used to reduce the Stark broadening data were those reported by Griem,<sup>26</sup> assuming a plasma temperature of 10 000 K, which is appropriate for the delay times and laser pulse energy used.<sup>25</sup> The inversion of electron densities from Stark widths is rather insensitive to temperature, as related to the corresponding reduced line widths. Nonetheless, to assess sources of error due to temperature uncertainty in the present data, the measured Stark line widths were also inverted using a temperature of 20 000 K and the corresponding fractional half-widths. Accordingly, the uncertainties reported with the measured free electron densities in Table 1 represent the maximum error associated with the uncertainty of 10 000 K and the uncertainty associated with the measured line width ( $\sim 0.02$  nm). This analysis revealed that the free electron densities were statistically identical ( $\sim 1 \times 10^{17}$  cm<sup>3</sup>) for all five analyte sources as well as for the baseline DI water case (see Table 1), indicating no fundamental changes in this parameter with the various carbon species.

To corroborate the invariance of plasma state, independent measurements of plasma temperature were made using a ratio of the  $N_2^+$  (first negative system) emission lines at 375.95 and 391.5 nm based on the method reported by Laux et al.<sup>27</sup> The results are also summarized in Table 1, and as with the electron density results, no significant difference in the plasma temperature is observed among the five analyte cases. It is noted that the calculated temperatures are considerably lower than 10 000 K used for the Stark broadening; however, the molecular spectra were recorded between 40 and 100  $\mu$ s following plasma initiation, which was necessary to capture the molecular emission. In concert, the electron density measurements, the plasma temperature measurements, and the excellent scaling of the plasma continuum emission all support a consistent and invariant plasma over the range of experimental conditions for all analyte species.

In addition to the carbon response as measured with the 247-nm atomic emission line, it is also useful to consider additional carbon-related emission bands. Specifically, if the differences in analyte response observed with the 247-nm line are the result of differences in the amount of atomic carbon generated within the plasma volume, then one might expect a similar trend with other carbon emission features such as those from CN. Measurements of the CN violet system ( $B^2\Sigma - X^2\Sigma$ ) have been widely observed in laser-induced plasmas and have been used for quantitative analysis.<sup>11,16</sup> In the current study, measurements of the CN violet band were performed and analyzed using the 388.3- (0,0) and 387.1-nm (1,1) emission lines. Representative background-subtracted (using DI water only) CN emission spectra are shown in Figure 4. The P/B values were calculated for the two lines as described above and then averaged to quantify the CN emission, with the results summarized in Table 1 for all five carbon analyte sources. Analysis of the CN emission data reveals a trend that is in agreement with the analyte response observed with the carbon atomic line, namely, a significant reduction in analyte signal when comparing the gas-phase species to the solid-phase species. The primary differences between the atomic carbon and CN emission

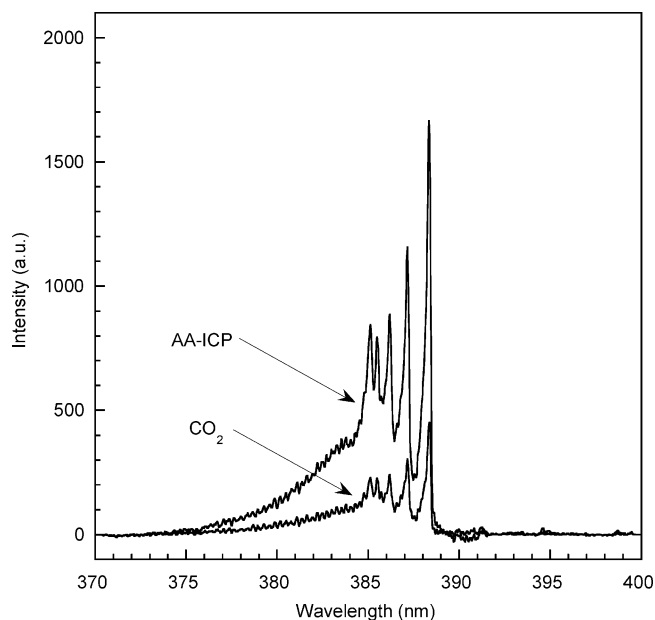


**Figure 4.** LIBS spectra in the vicinity of the CN violet system for the AA-ICP and  $CO_2$  analyte sources. The curves have been background-subtracted using the deionized water spectrum as a blank. All spectra have the same scale.

results are (i) that the ratios of the various solid-phase to gas-phase P/B values were reduced by a factor of  $\sim 2$  (ii) and that while the CN emission response of the  $CO_2$  and CO experiments was consistent, the CN response of the  $CH_4$  experiment was  $\sim 50\%$  greater than the  $CO_2$  and CO results.

## DISCUSSION

In aggregate, the above results clearly support a significant effect of the analyte state (i.e., solid vs gas phase) on the resulting analyte response, as measured by the corresponding analyte emission peaks. The similar response of the 247-nm carbon atomic emission line for all three gas species (which have markedly different C–H–O ratios), coupled with the identical free electron densities and temperature for all plasma conditions, lead to the conclusion that the observed differences in analyte response are not the result of differences within the plasma following dissociation (i.e., not emission quenching or analyte recombination effects). In contrast, the differences in analyte response are concluded to arise from differences in the amount of analyte originally dissociated to atomic carbon within the laser-induced plasma volume. To discuss the proposed reasons for such a disparity in analyte dissociation, it is first necessary to consider in more detail the nature of the solid-phase carbon and the overall role of particulates in laser-induced plasmas.

The nebulizer system used in the current experiments was investigated in detail in a previous study.<sup>23</sup> In that earlier work, AA-ICP grade solutions of iron and titanium were nebulized under conditions essentially identical to the present study. The resulting solid particulates were collected and analyzed using TEM. The particles produced following desolvation (i.e., particles at the LIBS sample point) were found to group about a mean particle size less than 100 nm and, as expected, were found to scale with the mass concentration of analyte in the nebulized solution. Based on this earlier study, the current nebulization of solutions of carbon as

(27) Laux C. O.; Gessman R. J.; Kruger C. H.; Roux F.; Michaud F.; Davis S. P. *J. Quant. Spectrosc. Radiat. Transfer* **2001**, *68*, 473–482.

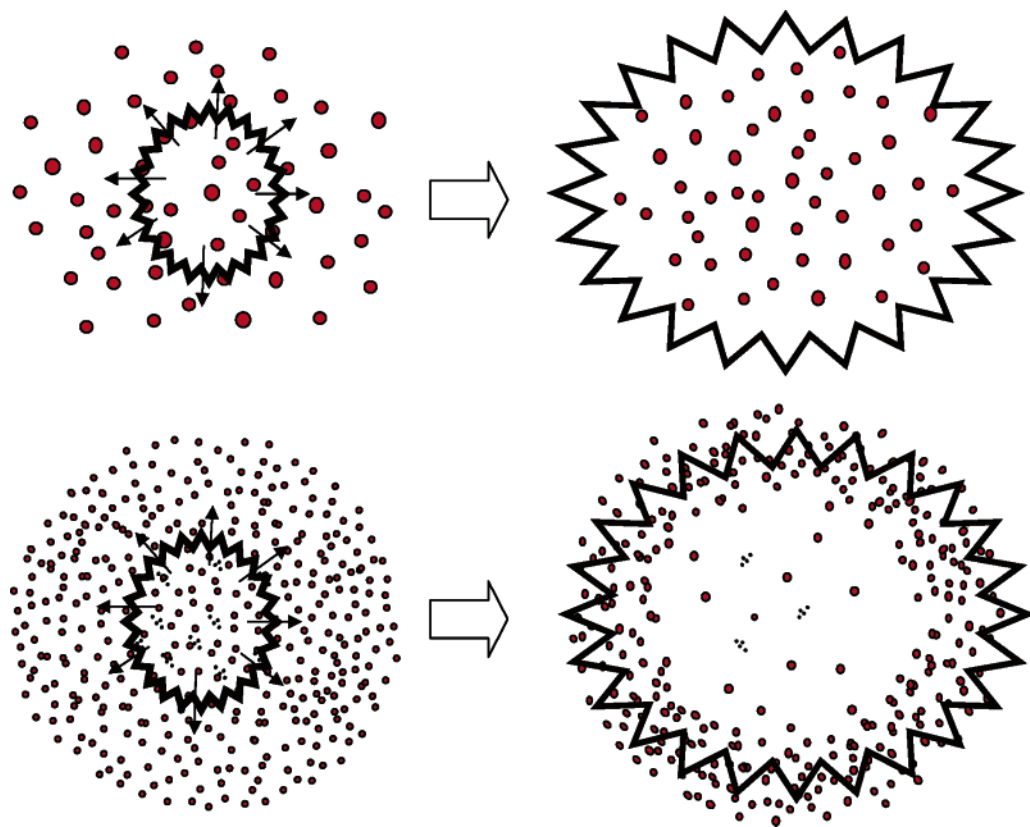


**Figure 5.** Schematic detailing the proposed interactions between the rapidly expanding plasma wave and the analyte species. Large particulates or aerosols (upper image pair) are shown to resist outward radial transport by the plasma wave, whereas nano-scale (e.g., gas phase) analyte species (lower image pair) will tend to be depleted from the plasma core.

oxalic acid over the range of 500–5000  $\mu\text{g}$  of C/mL is expected to produce carbon-rich aerosols primarily in the size range from about 50 to 100 nm. Qualitative light scattering measurements through the LIBS sample chamber revealed the presence of a uniform aerosol cloud of similar scattering intensity for both the AA-ICP and 30-nm PS experiments. This pronounced uniform scattering was absent with the three gas-phase carbon species. The chemical nature of the submicrometer-sized aerosols created from nebulization of the AA-ICP solutions was not determined, but it is expected that the particles would be rich in oxalic acid, which takes the form of a transparent, colorless crystal in the solid phase. TEM analysis of the 30-nm PS suspension particles confirmed a mean size of 28 nm with a relative standard deviation of  $\sim 16\%$ .

Assuming that gas molecules have an effective size on the order of 1 Å, there was a pronounced range of length scales realized with the three groups of analyte species:  $\sim 0.1$  nm for the gas-phase species,  $\sim 30$  nm for the polystyrene particles, and  $\sim 100$  nm for the nebulized AA-ICP standards. It is noted that this entire size range falls well below a previously established  $\sim 2\text{-}\mu\text{m}$  upper size limit for complete dissociation of silicon oxide particulates in a comparable laser-induced plasma;<sup>28</sup> hence, the current results support the earlier conclusion that the varied analyte response is not the result of incomplete dissociation *within the plasma* stemming from particle size effects. As an alternative, it is proposed that a physical mechanism is in effect that selectively (i.e., dependent on analyte state) perturbs the analyte species

during plasma formation and growth, thereby affecting the resulting amount of analyte present within the subsequent laser-induced plasma.

Such a mechanism must selectively remove molecular species from within the resulting plasma volume to account for the analyte response data observed in this study. In addition, one would expect the depletion of molecular species to be combined with a secondary size effect, such that solid-phase species preferentially remain within the plasma volume in a manner that scales with particle size or mass. Previous measurements of the plasma volume using a temporal probe laser revealed that the laser-induced plasma grew from its initial breakdown volume (i.e., laser focal volume) to an effective plasma volume of  $\sim 1\text{ mm}^3$  over a time scale of  $\sim 20\text{ ns}$ .<sup>29</sup> One may consider that the rapidly expanding plasma can be thought of as a shockwave-like phenomenon, in which the highly energetic pressure and electron wave rapidly expands from the original plasma kernel. As the plasma wave expands, molecular and particulate species are pushed toward the edge of the plasma volume. However, due to the many orders of magnitude difference in the mass of gas-phase species (molecules) and solid-phase species (particulates), it is expected that the efficiency at which a given species is carried by the plasma wave will scale inversely with particle mass. In other words, an effective analyte *slip factor* will exist as the plasma wave expands. A schematic of this proposed effect is presented in Figure 5. Within such a model, analyte species at the molecular level would tend to be selectively swept out of the plasma core toward

(28) Carranza, J. E.; Hahn, D. W. *Anal. Chem.* **2002**, *74*, 5450–5454.

(29) Carranza, J. E.; Hahn, D. W. *J. Anal. At. Spectrosc.* **2002**, *17*, 1534–1539.

the plasma edges, where temperatures and electron densities are significantly lower. Analyte species at the particulate scale would be less affected by these drag forces due to inertial effects and would therefore selectively remain in the plasma core volume, leading to more complete dissociation and therefore a greater effective analyte concentration and emission response. Previously reported experiments using laser-induced fluorescence to image LIBS plasmas in the presence of gold aerosols and particulates appear to support such a phenomenon.<sup>30</sup>

Based on this working model, it is expected that a finite particle size (i.e., mass) exists where the efficiency of remaining within the plasma core reaches a plateau, essentially the point in which all such particulates effectively remain within the core plasma volume. While determination of such a particle size requires further validation of the hypothesis itself, as well as additional experimental work and modeling, it is useful to consider some limiting values based on the available data. A linear analyte response was observed for silicon oxide particles over the size range of 1–2.1  $\mu\text{m}$ , as reported previously.<sup>28</sup> Hence 1  $\mu\text{m}$  may be considered an upper limit for the estimated particle size necessary to minimize analyte depletion within the plasma volume. Based on the current study, particle size effects are concluded to exist over the 30–100-nm size range. Accordingly, one may reasonably conclude that the critical size for an analyte species such that

(30) Nakata, Y.; Okada, T. *Appl. Phys. A* **1999**, *69* (Suppl.), S275–S278.

(31) Schoolcraft, T. A.; Constable, G. S.; Zhigilei, L. V.; Garrison, B. J. *Anal. Chem.* **2000**, *72*, 5143–5150.

(32) Lushnikov, A. A.; Negin, A. E. *J. Aerosol Sci.* **1993**, *24*, 707–735.

(33) Gornushkin, I. B.; Kazakov, A. Y.; Omenetto, N.; Smith, B. W.; Winefordner, J. D. *Spectrochim. Acta, Part B* **2004**, *59*, 401–418.

preferential removal from the plasma core is minimized is in the range of 0.1–1  $\mu\text{m}$ . Particles above this range are expected to display a linear analyte response (i.e., no particle size effect) up to the limit for complete vaporization. Particles below this range, including down to the molecular regime, are expected to display significant size effects with respect to the analyte response.

Overall, the range of data reported in the current study supports the conclusion that there is preferential accumulation and dissociation of solid-phase analyte species within the plasma center resulting in an enhanced analyte response, as measured by atomic and molecular emission, as compared to gas-phase analytes. It is proposed that such an effect is realized by the interaction of the analyte species (solid or gas phase) with the expanding plasma, with relative inertial effects playing a key role. To date, published studies have explored the interaction of aerosols in laser-induced plasmas,<sup>31–33</sup> however, the coupling of such interactions, including particle dynamics and plasma emission processes, remains an ongoing issue. An important outcome of this study is demonstration of the need to produce calibration schemes for use with LIBS that reflect as much as possible the physical state of the analyte species of interest.

#### ACKNOWLEDGMENT

This work was supported in part by the National Science Foundation through Grant CTS-0317410.

Received for review September 23, 2004. Accepted November 22, 2004.

AC048587D